Measured and simulated ^{252}Cf(sf) prompt neutron-photon competition

Matthew J. Marcath,[1,*] Robert C. Haight,[2] Ramona Vogt,[3,4] Matthew Devlin,[2] Patrick Talou,[2] Ionel Stetcu,[2] Jørgen Randrup,[5] Patricia F. Schuster,[1] Shaun D. Clarke,[1] and Sara A. Pozzi[1]

[1]*Department of Nuclear Engineering and Radiological Sciences, University of Michigan, Ann Arbor, Michigan 48109, USA*

[2]*Los Alamos National Laboratory, Los Alamos, New Mexico 87545, USA*

[3]*Physics Division, Lawrence Livermore National Laboratory, Livermore, California 94551, USA*

[4]*Physics Department, University of California, Davis, California 95616, USA*

[5]*Nuclear Science Division, Lawrence Berkeley National Laboratory, Berkeley, California 94720, USA*

(Received 23 January 2018; published 30 April 2018; corrected 22 May 2018)

Neutrons and photons are characteristically emitted during the nuclear fission process when a deformed, neutron-rich nucleus divides into two fragments that then deexcite. During deexcitation, neutrons are emitted first, followed by photons; this process gives rise to correlated emissions. Few data exist on event-by-event neutron-photon correlation. In this work, ^{252}Cf(sf) neutron and photon correlations were measured with an array of 45 liquid organic scintillation detectors and a fission chamber. The measured correlations are compared with `MCPNX-PoliMi` simulations using the built-in model and two event-by-event fission models, `CGMF` and `FREYA`, which predict correlations in prompt emissions from fission. Experimental results suggest weak neutron-photon competition during fragment deexcitation.

DOI: 10.1103/PhysRevC.97.044622

I. INTRODUCTION

In nuclear fission, neutrons are primarily emitted first [1] followed by photon emission [2]. However, the details of the transition from neutron to photon emission are poorly understood. This work seeks to observe and quantify the competition between neutron and photon emission in ^{252}Cf(sf). Many studies of prompt emissions, exclusive to one particle type, such as neutrons alone, have been done for key fissioning isotopes [3–11], but only a few experiments [12–15] have measured neutrons and photons simultaneously. In previous work, experiments were performed to correlate both neutron and photon emission with fragment properties. One [12] shows a positive correlation, another [13] observes a complex fragment-dependent correlation, a third [14] reports a negative correlation, while a fourth [15] found no evidence of correlated emission from specific fragment pairs. The fission event models `CGMF` [16–19] and `FREYA` [20–26], however, predict a negative correlation. Additionally, only one previous experiment [14] commented on event-by-event correlations; the neutron and photon multiplicity from each fission event was measured and a correlation between the neutron and photon multiplicities was observed. Given the contradictory experimental results, it is clear that the transition from neutron emission to photon emission in fission fragment deexcitation is not well understood or measured.

After fission occurs, during fragment deexcitation, neutrons are primarily emitted until the fragment excitation energy nears the neutron separation energy [27]. Neutrons remove much of the excitation energy, but do little to change the angular momentum. Photons are emitted primarily after neutron emission and, in general, decrease the fragment angular momentum [28]. The transition between neutron and photon dominance could give rise to correlations between them, as were previously measured [12–15].

Recently, physics-based event-by-event models, capable of calculating neutron and photon correlations, were developed to move beyond empirical models [29–31] and models limited to single-particle distributions [32,33]. These models include `CGMF` [16–19], `FREYA` [20–26], `FIFRELIN` [34], and `GEF` [35]. These event-by-event models follow pairs of fission fragments from scission through the complete deexcitation process, capturing correlations between emitted neutrons, photons, and fragments. Many measured data sets are available to validate single-particle distributions from these event-by-event models, but few correlated neutron-photon data sets exist and are currently limited to ^{252}Cf(sf) [12–15]. Correlated data are particularly useful to validate the event-by-event treatment of the transition from neutron emission to photon emission.

This work presents measured neutron-photon correlations event-by-event. Neutrons and photons from ^{252}Cf(sf) were measured with an organic scintillator array. The measured neutron-photon correlations are compared to simulations employing the `CGMF` [16–19], `FREYA` [20–26], and `MCPNX-PoliMi` [29,30] fission generators. Here, the built-in `MCPNX-PoliMi` fission model source card option `IPOL(1)` $= 1$ is referred to as `POLIMI` in the following. `MCPNX-PoliMi` was used to model the laboratory geometry and to transport fission neutrons and photons provided by three fission event generators. This work is the first dedicated measurement of neutron-photon correlations from all fragments on a fission-by-fission basis and provides new insight into neutron-photon competition.

*mmarcath@umich.edu

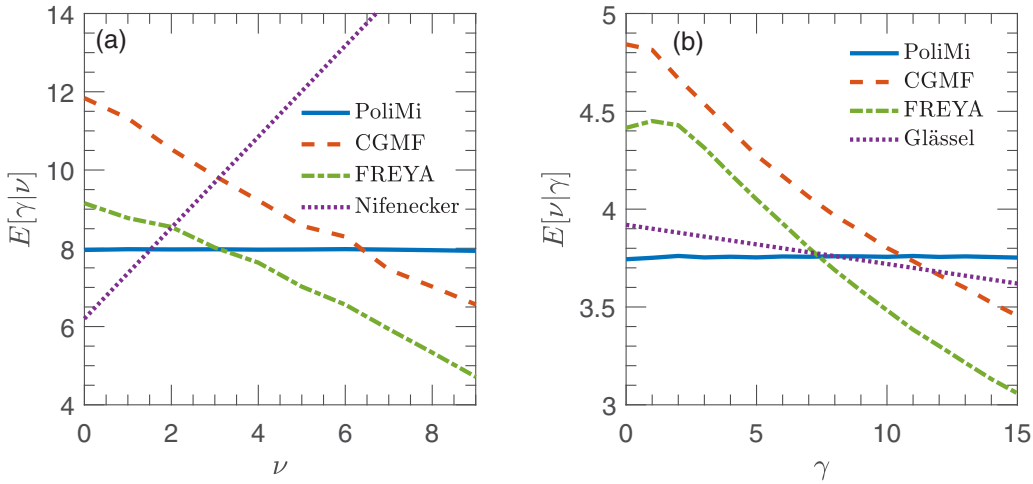

FIG. 1. The average number of photons emitted given neutron number, $E[\gamma|\nu]$ (a), and average number of neutrons emitted given photon number, $E[\nu|\gamma]$ (b), for ^{252}Cf(sf). Results from fission models are compared to data from Nifenecker *et al.* [12] (a) and from Glässel *et al.* [14] (b).

II. PREVIOUS MEASUREMENTS OF NEUTRON-PHOTON CORRELATIONS

The four previous experiments measuring ^{252}Cf(sf) neutron-photon correlations discussed in the Introduction [12–15] are described in more detail in this section. Nifenecker *et al.* explored the correlation as a function of fragment mass [12]. Wang *et al.* studied the correlation in fragment mass and in kinetic energy bins [13]. Glässel *et al.* determined the correlation as a function of fragment kinetic energy as well as on an event-by-event basis [14]. Bleuel *et al.* isolated event-by-event multiplicities for two sets of fragment pairs [15].

Nifenecker *et al.* [12] averaged photon and neutron measurements over fragment properties. Therefore this experiment cannot comment on the event-by-event nature of neutron and photon competition. They concluded, however, that there was a linear relationship between the average total photon energy, $\overline{E}_\gamma$, and the average number of neutrons emitted for a given fragment, $\overline{\nu}$, in a ^{252}Cf(sf) event $\overline{E}_\gamma(A,\mathrm{KE}) = [0.75\overline{\nu}(A,\mathrm{KE}) + 2]$ MeV, where A is the fragment mass number and KE is the fragment kinetic energy. When averaged over a pair of complementary fragments, they reported a relationship between total photon energy and neutron multiplicity of $\overline{E}_\gamma^{\mathrm{tot}} = [0.75\overline{\nu} + 4]$ MeV. They further determined a relationship between photon and neutron multiplicity emitted per fragment of $M_\gamma = 1.13\overline{\nu} + 3$ assuming a proportionality of 1.55 photons per MeV based on the measurements of prompt [36] and delayed [37] photons, $M_\gamma(A)$, summed by John *et al.* [38]. They suggested that their positive correlation is evidence of an increase in the mean spin of the fragments with excitation energy, while the excitation energy is determined from measured fragment masses and total kinetic energy. Other modes of fragment excitation are ignored in their discussion.

The Nifenecker *et al.* correlation is shown in Fig. 1(a), where $E[\gamma|\nu]$ is the expected number of photons emitted given the number of neutrons emitted. If the neutron and photon multiplicity probability matrix is $P(\nu,\gamma)$, then $E[\gamma|\nu]$ is the row average while $E[\nu]$ is the average ν over the entire $P(\nu,\gamma)$ matrix.

Wang *et al.* [13] expanded upon the study in Ref. [12] by correlating photon and neutron multiplicities with total kinetic energy over three fragment mass regions of interest: light ($85 < A < 123$), symmetric ($124 < A < 131$), and heavy ($132 < A < 167$). The light and symmetric mass regions exhibit a linear trend with a positive slope, qualitatively consistent with Ref. [12], whereas the heavy region is nonlinear with an overall positive trend. Wang *et al.* also showed that the FREYA results followed general trends of the measured neutron-γ correlation binned in fragment mass and total kinetic energy (TKE), but the overall agreement was poor. While FREYA shows a fragment-dependent, positive correlation following the experimental binning, this result is not indicative of the ability of FREYA to reproduce observed neutron and photon competition on a fission-by-fission basis.

On the other hand, Glässel *et al.* [14] studied correlations between neutron and photon multiplicities on a fission-by-fission basis as well as based on averages such as studied by Nifenecker *et al.* When studying averages, they determined that the photon multiplicity distribution as a function of fragment mass, $M_\gamma(A)$, was rather independent of mass, in contradiction to the earlier results of John *et al.* [38]. Thus, rather than the 1.13 photons per neutron obtained by Nifenecker [12], given above, they found ∼0.16 photons emitted per neutron, a much smaller result. In addition, in event-by-event mode, they determined a decrease in $\overline{\nu}$ of 0.02 per emitted photon, suggesting that neutron multiplicity and photon energy are anticorrelated. While they also suggest, like Nifenecker, that a positive correlation with respect to excitation energy is evidence of an increase in the mean fragment spin with excitation energy, they add the qualification that this conclusion does not have any bearing on neutron-photon competition.

The Glässel *et al.* correlation is shown in Fig. 1(b), where $E[\nu|\gamma]$ is the expected number of neutrons emitted given the number of emitted photons. For the probability matrix $P(\nu,\gamma)$, $E[\nu|\gamma]$ is the column average while $E[\gamma]$ is the average γ over the entire $P(\nu,\gamma)$ matrix.

Bleuel *et al.* [15] found no significant correlation between neutron and photon multiplicity. Using a high-efficiency photon detector and known γ-ray energy transitions, they isolated the photon multiplicity distributions for two post-neutron emission fragment pairings: two-neutron ^{106}Mo + ^{144}Ba and four-neutron ^{106}Mo + ^{142}Ba. The two-neutron distribution yielded 9.9 ± 0.7 photons on average while the four-neutron distribution yielded an average of 9.9 ± 0.5 photons. In contrast, Nifenecker *et al.* would predict an increase of $\sim$1.3 photons for the four-neutron distribution relative to that of two neutrons, an effect which should have been detectable. The Bleuel *et al.* conclusion was, however, based on specific fragment pairs with prominent photon lines rather than averages. It was also limited statistically, giving large uncertainties in the measured multiplicities.

The work presented here focuses on observing neutron-photon correlations on an event-by-event basis rather than averaged over fragment mass or energy to investigate event-by-event competition. We seek to determine if the number of photons detected, γ', in a given fission event has any implication on the number of neutrons detected, ν'.

III. FISSION MODELS

Three fission models were used in this work: the built-in `MCPNX-PoliMi` (referred to as `POLIMI`), `CGMF`, and `FREYA`. See Ref. [40] for more details and model comparisons. The discussion here is focused on event-by-event neutron and photon correlations.

The general purpose transport code `MCPNX-PoliMi` [29,30] was used to transport particles from all three fission models. The `POLIMI` spontaneous-fission source uses evaluated multiplicity distributions and energy spectra for prompt neutrons and photons [30]. Because neutrons and photons are sampled independently, no correlation between particle types is predicted. However, neutrons are correlated with the sampled fission fragment direction in the laboratory frame because of the fragment momentum boost.

The `CGMF` code [16–19], developed at Los Alamos National Laboratory, is a Monte Carlo implementation of the statistical Hauser-Feshbach nuclear reaction theory. As input, `CGMF` takes fragment mass, charge, and total kinetic energy (TKE) yields as well as ground-state masses to calculate excitation energies. The code follows the fission fragments immediately after scission through deexcitation by sequential neutron and photon emission. `CGMF` uses a mass-dependent parameter to better reproduce the experimental mass-dependent neutron multiplicity and uses a single parameter to fix the initial fragment spin distribution. Because Hauser-Feshbach nuclear reaction theory is used, both neutrons and photons could be emitted during any stage of the deexcitation process. However, as the fragment deexcites, photon emission becomes more likely. The calculated neutron-photon competition is strongly influenced by the spin distribution in each fragment produced. A higher spin leads to more photons being emitted at the expense of emitted neutrons.

`FREYA` v2.0.2 (Fission Reaction Event Yield Algorithm), developed at Lawrence Berkeley and Lawrence Livermore National Laboratories, calculates emissions from complete

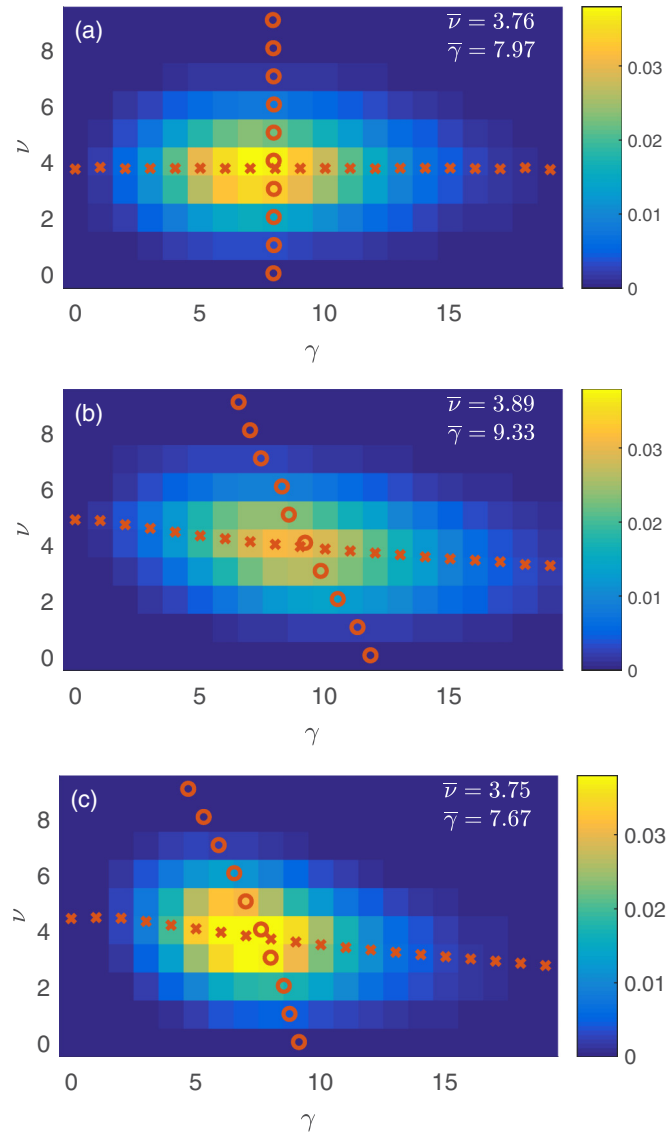

FIG. 2. ^{252}Cf(sf) neutron (y-axis) and photon (x-axis) multiplicities with mean neutron, $\overline{\nu}$, and mean photon, $\overline{\gamma}$, multiplicities from `POLIMI` (a), `CGMF` (b), and `FREYA` (c) with $E[\nu|\gamma]$ (x) and $E[\gamma|\nu]$ (o) overlaid.

fission events on an event-by-event basis [20–26]. Similar to `CGMF`, `FREYA` requires fragment mass and charge yields as inputs as well as tabulated ground-state masses. `FREYA` also requires the fragment TKE as a function of heavy fragment mass rather than the yields as a function of TKE, as in `CGMF`. Like `CGMF`, `FREYA` uses a single parameter to modify the initial spin distribution. As opposed to `CGMF`, `FREYA` currently uses a single, fixed parameter to determine fragment excitation energy sharing. Neutron evaporation occurs until the nuclear excitation energy is at or below the neutron separation energy where photon emission takes over. `FREYA` produces negatively correlated neutron and photon multiplicities, like `CGMF`.

In Figs. 1 and 2, the calculated distributions for neutron and photon emission from ^{252}Cf(sf) are shown for `POLIMI`, `CGMF`, and `FREYA`. There is no correlation between neutrons and photons with `POLIMI`. Both `CGMF` and `FREYA`, however, exhibit

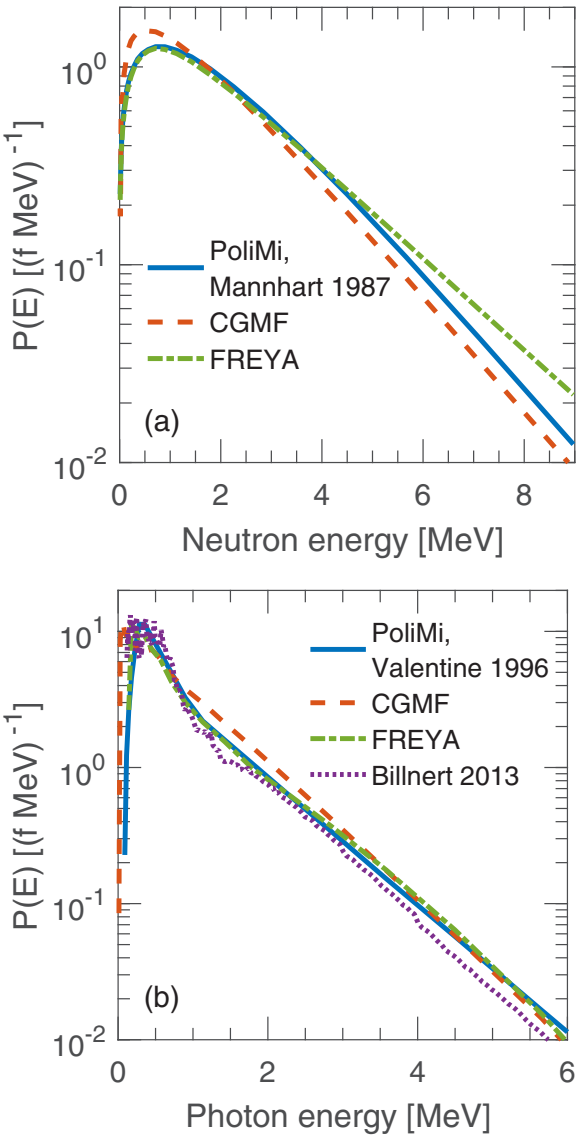

FIG. 3. ^{252}Cf(sf) neutron (a) energy spectra from POLIMI (uses Mannhart [39]), CGMF, and FREYA. ^{252}Cf(sf) photon (b) energy spectra from POLIMI (uses Valentine *et al.* [31]), CGMF, FREYA, and Billnert *et al.* [9].

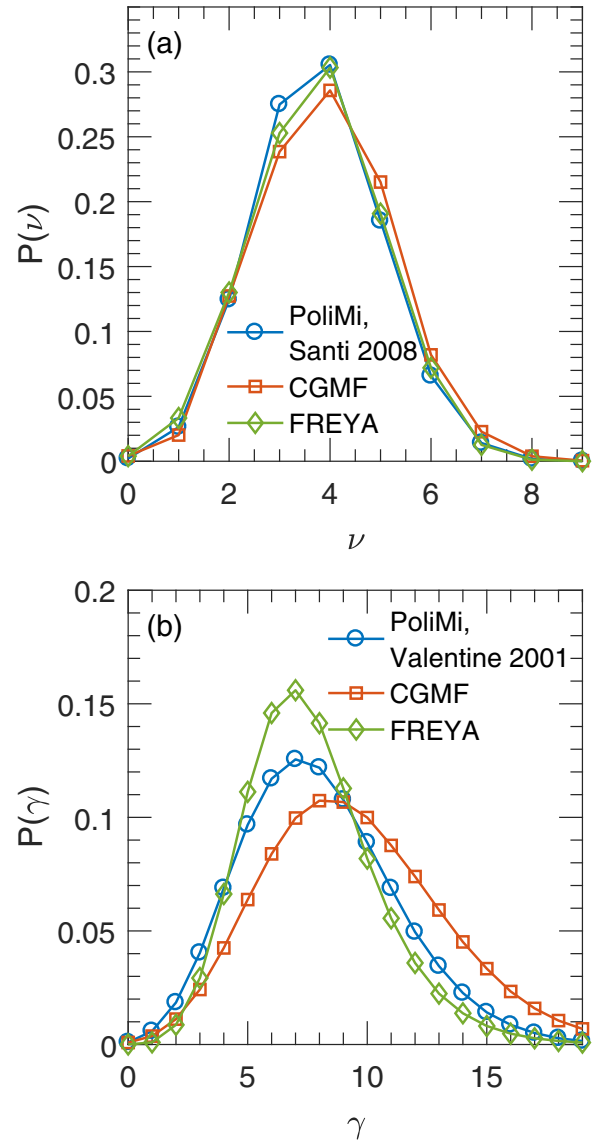

FIG. 4. ^{252}Cf(sf) neutron (a) multiplicity distributions from POLIMI (uses Santi and Miller [4]), CGMF, and FREYA. ^{252}Cf(sf) photon (b) multiplicity distributions from POLIMI (uses Valentine *et al.* [33]), CGMF, and FREYA.

similar negative correlations between the particle multiplicities on a event-by-event basis, as shown in Fig. 1. The trends from these two calculations are the same even though the absolute scales are different.

In Fig. 3, the fission model neutron and photon energy spectra are compared. POLIMI uses the Mannhart [39] ^{252}Cf(sf) neutron energy spectrum evaluation, shown in Fig. 3(a). The calculated CGMF ^{252}Cf(sf) neutron spectrum is softer than the evaluation spectrum, Mannhart [39], whereas the calculated FREYA spectrum is harder. The photon spectra, in Fig. 3(b), are compared to an experiment by Billnert *et al.* [9]. POLIMI uses the Valentine [31] ^{252}Cf(sf) photon evaluation, shown in Fig. 3(b). Above 1 MeV, all calculated photon spectra are harder than the Billnert *et al.* data. The POLIMI and FREYA photon spectra are in agreement with each other, but the CGMF spectrum is slightly higher between 1 and 3 MeV.

In Fig. 4(a), the fission model neutron and photon multiplicity distributions are compared. POLIMI uses the Santi and Miller [4] evaluation for its ^{252}Cf(sf) neutron multiplicity distribution. Reflecting the mean neutron multiplicities shown in Fig. 2, the POLIMI and FREYA neutron multiplicity distributions are similar while CGMF shows a slightly higher distribution. A more recent version of CGMF now computes $\bar{\nu}$ at 3.76, without modifying the neutron-photon correlation as discussed in the present work. POLIMI uses Valentine and Mihalczo [33] for its ^{252}Cf(sf) photon multiplicity distribution. While the POLIMI and FREYA mean photon multiplicities are similar, shown in Fig. 2, the FREYA distribution is narrower than the POLIMI distribution. The CGMF photon multiplicity distribution is significantly higher than the other data.

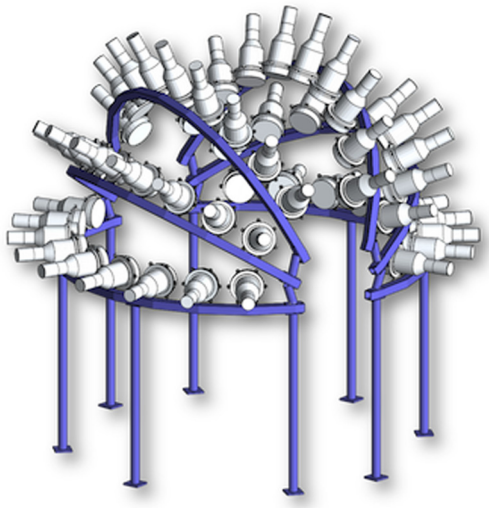

FIG. 5. A model of the Chi-Nu detector holder and the 45 17.78 × 5.08 cm EJ-309 detectors. Fifty-four detectors are pictured. One of the topmost arcs was in place but its signals were not read out. The fission chamber was placed at the center of the hemisphere for the measurement.

IV. EXPERIMENTAL METHOD AND ANALYSIS

We measure correlations between neutrons and photons emitted during spontaneous fission of ^{252}Cf. First we describe the experiment and the data acquisition. Then we discuss correlated background subtraction. Finally, we present simulations of the experiment.

A. Experiment

The Los Alamos National Laboratory Chi-Nu array [41], consisting of 54 17.78 cm diameter by 5.08 cm thick cylindrical EJ-309 scintillators coupled to 12.7 cm diameter photomultiplier tubes (Hamamatsu R4144), was used to measure neutrons and photons from ^{252}Cf(sf). In this work, because of the number of data channels available in the electronics, only 45 of the detectors were used. The array, shown in Fig. 5, has a flight path of 100 cm from each detector to the fission chamber, located at the center of the hemispherical array.

This experiment used an ionization chamber designed and fabricated in 2010 at Oak Ridge National Laboratory (ORNL) [42]. The californium source, with the composition shown in Table I, was deposited over a hemispherical surface in the chamber. In a fission event, one or two fragments escape the surface and deposit energy through ionization, producing a pulse above a fixed threshold set to exclude α-particle interactions [43]. The chamber was positioned in the center of the array on the end of a metal tube. The ionization chamber signal was used as the fission time trigger.

TABLE I. The californium source composition and the fission rates from the sources on the date of assay, November 2010, and the date of the experiment, July 2015.

Isotope	Nov. 2010 Assay (μg)	Nov. 2010 Fiss. Rate (f/s)	July 2015 Fiss. Rate (f/s)
^{252}Cf	1.641	9.705×10^5	2.986×10^5
^{250}Cf	0.265	8.19×10^2	6.45×10^2
^{248}Cm	0.173	3.06	17.5

The experiment was performed shortly after the production of the californium fission chamber relative to the 2.6 year ^{252}Cf half-life. Therefore the ^{252}Cf(sf) rate was high relative to spontaneously fissioning impurities in the sample, as we now describe. The fission rate at the time of measurement was 2.98×10^5 spontaneous fissions per second. The majority of those fissions are ^{252}Cf [44] with small contributions from ^{250}Cf(sf) (0.2%) and ^{248}Cm(sf) (6×10^{-5}%). The different decay rates result in a growing fraction of ^{250}Cf and ^{248}Cm relative to ^{252}Cf. However, the fission contributions from ^{250}Cf(sf) and ^{248}Cm(sf) are negligible and are thus ignored in further analysis.

The fission rate in the ionization chamber was low enough that the fission events and their emissions are assumed to be well separated in time. The pile-up of fission events was approximately 3.5%, given the source rate and a 150 ns window; long enough to acquire neutrons at and below the detector threshold energy. The fission chamber pulse height trigger threshold, however, was set for zero digitizer dead time, resulting in a trigger rate of 65% of the expected fission rate. There were 3.21×10^9 fission triggers above threshold during the experiment.

Pulses from the detectors and fission chamber were digitized using three CAEN V1730 waveform digitizers with 500 MHz sampling and 14-bit amplitude resolution over a 2 V range. The detectors were gain-matched to 478 keVee (where "ee" denotes electron equivalent) at 0.3 V with a lower threshold of 40 keVee (a 0.62 MeV proton recoil equivalent threshold) and an upper threshold of 3180 keVee (an 8.1 MeV proton recoil equivalent threshold) determined by the upper limit of the 2 V range. All digitized waveforms were recorded for post-processing. Pulse shape discrimination (PSD) was used to discriminate between neutron and photon events in the liquid organic scintillators [45,46].

For the organic scintillators, only pulses above a 100 keVee lower threshold (the 0.80 MeV proton recoil equivalent threshold) were analyzed. Double-pulse fractional cleaning [47] was used to remove pile-up events. Pulse pile-up is removed because the PSD algorithm does not handle that case; pile-up pulses are usually classified as a neutron regardless of the contributing particle types. After cleaning, charge integration PSD [48] was performed. In charge integration PSD, two integrals are computed: one over the whole waveform and one over the tail of the waveform. The tail integral starts 24 ns after the peak. A quadratic PSD line was assigned to discriminate between the two particle types using an algorithm described by Polack *et al.* [48]. Figure 6 shows the tail integral plotted against the total integral. Two bands are produced, one for photons (below the discrimination line) and one for neutrons (above the discrimination line). Significant overlap occurs at small total integrals (below ∼0.5 V ns) and pulse heights (below ∼0.1 MeVee). Therefore, misclassification is most likely in this region. Misclassification of photons as

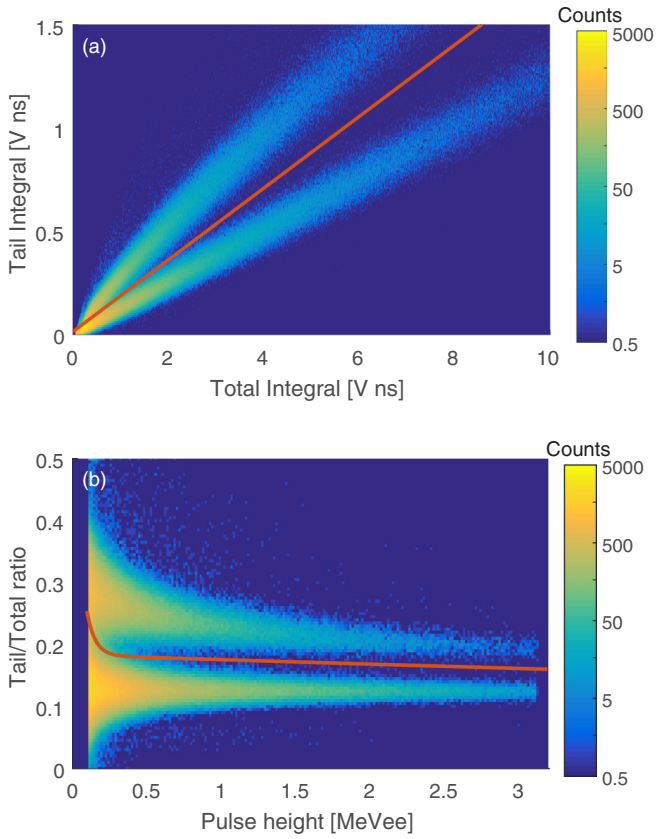

FIG. 6. (a) The tail integral as a function of the total waveform integral. (b) The tail-to-total ratio as a function of pulse height. Two features are apparent: the upper bands in each panel primarily includes neutron detections while the lower bands indicate photon detections, separated by the discrimination line, in red. More than 730 000 detections are shown.

neutrons was estimated to be ∼1% using time of flight. After background is subtracted in the time region from fission to 10 ns after the fission, only photon detections are expected and all neutron detections in that region were considered misclassified photons.

The organic scintillators, in this configuration, were sensitive to neutrons above 0.8 MeV, given a 100 keVee threshold, and had limited sensitivity to neutrons above 8.1 MeV. The detectors are sensitive to approximately 77% of the neutron spectrum with an intrinsic efficiency of ∼32% for the full spectrum. The detectors are sensitive to the full prompt photon spectrum. The intrinsic efficiency to the full photon spectrum is approximately 23%. Obtaining the correlation between the emitted neutron and photon multiplicities using experimental data was not possible because the inverse problem is poorly posed given the low neutron and photon efficiencies. While organic scintillators are sensitive to most of the photon and neutron spectra, these detectors are not uniformly sensitive to the entire spectral energy distribution. Consequently, correlations in regions where the detectors are less sensitive may be unobserved or less proportionately observed.

After post-processing of the waveforms, which includes particle identification based on PSD, neutron and photon events in a 400 ns coincidence window were collected. The coincident events were analyzed to produce pulse height, cross-correlation, multiplicity, and time-of-flight distributions. The experimental distributions were then compared to simulated results from the fission models employed.

B. Correlated background subtraction

The simple assumption in a single bin experiment, such as the neutron multiplicity as a function of fragment mass, that the measured signal is a simple sum of real and accidental counts, does not hold for these data. Instead, we have a two-dimensional histogram of measured events, M, with each element of the histogram, $m_{i,j}$, having two indices: i for the number of detected neutrons and j for the number of detected photons in each event. Each element $m_{i,j}$ is a sum of contributions from a combination of the real, R, and the accidental, A, histograms with elements $r_{k,l}$ and $a_{i-k,j-l}$ respectively,

$$m_{i,j} = \sum_{k=0}^{i} \sum_{l=0}^{j} r_{k,l} a_{i-k,j-l} \tag{1}$$

The one-dimensional background subtraction method used by Diven *et al.* [49] is extended here to two dimensions (neutrons and photons) to account for the accidental contributions to $m_{i,j}$.

Given $m_{i,j}$, it is possible to solve for the elements of unknown reals histogram $r_{i,j}$, with $(k,l) \neq (i,j)$:

$$r_{i,j} = \frac{m_{i,j} - \sum_{k=0}^{i} \sum_{l=0}^{j} r_{k,l} a_{i-k,j-l}}{a_{0,0}} \tag{2}$$

Due to the coincidence logic imposed at data acquisition (only events with one or more triggered detections were saved), the $m_{0,0}$ element could not be measured directly. However, $a_{0,0}$ was directly measurable. Thus, $m_{0,0}$ and $r_{0,0}$ were estimated from the simulation of the experiment. Section V A discusses the fidelity of the simulation compared to experiment.

C. Simulation

The `POLIMI` code was used to model the laboratory geometry and particle transport. `POLIMI` models the detector system and surrounding laboratory in great detail. The detectors are modeled to almost full detail; the photomultiplier tube electronics are partially homogenized. Ignoring small hardware such as bolts and nuts, the Chi-Nu array structure is fully modeled. The concrete floor was modeled to replicate room-return effects. One topmost detector arc was not used for data acquisition. However, it was left in place during the measurement and therefore was included in the model of the experiment.

The ORNL fission chamber is modeled in detail with the source term sampled over the 1 cm diameter spot on a 304L alloy stainless steel hemispherical surface.

The waveform processing and classification is assumed to be ideal in simulation; particle misclassification is not modeled. Misclassification is most prevalent at low pulse heights. Therefore, a conservative pulse height threshold of 100 keVee was used.

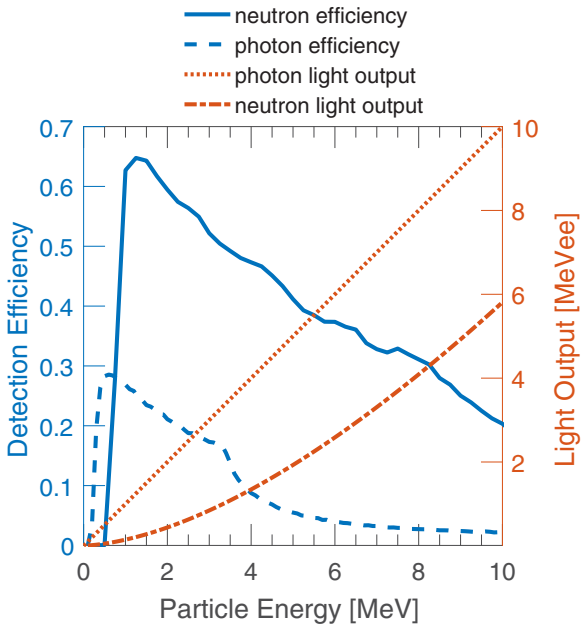

FIG. 7. Calculated neutron and photon detection efficiency and light output distributions used in the detector response code for neutron scattering on a proton and for photon scattering on an electron.

Other fission event generators were also utilized to generate events for transport. The fission event generators (CGMF, FREYA, and POLIMI) were used to produce a history file of fission events which were passed to the full POLIMI model for particle transport. Initial energy, initial direction, and particle type for each particle generated in each individual fission event were passed to POLIMI. The POLIMI code samples a new random fission event when using POLIMI and FREYA. A history file of 1.92×10^6 fission events generated by CGMF was resampled with new, randomly sampled, fission fragment directions.

Following transport, POLIMI records a file detailing interactions within specified detector cells. Details recorded in the interaction file include but are not limited to interaction type, particle type, nucleus of interaction, energy deposited, and time of interaction. This interaction file was passed to a code emulating detector response. The detector response code converts energy deposition to scintillation light, handles multiple interactions, and applies thresholds to ultimately record particle type, light output, and time for each detection. The light output distributions in MeV electron equivalent (MeVee) for energy deposited in MeV from neutron scattering on a proton and from a photon scattering on an electron are shown in Fig. 7. The Birks model, a semiempirical relationship described by Norsworthy *et al.* [50], was implemented in the detector response code to convert neutron energy deposited on protons to light output in the EJ-309 scintillator. The light output response from photon scattering on electrons was one-to-one. Using POLIMI and the detector response code, the simulated intrinsic efficiency was calculated as a function of incident particle energy and is shown in Fig. 7 for neutrons and photons. After detector response is applied, POLIMI simulation results from each ^{252}Cf(sf) event generator were compared to measurement.

V. RESULTS

Recall that three fission event generators (CGMF, FREYA, and POLIMI) were used to produce a history file of fission events which were passed to the full POLIMI model for particle transport. Initial energy, initial direction, and particle type for each particle generated in each individual fission event was passed to POLIMI for all fission event generators. Experimental and simulated detector results are compared for independent and dependent multiplicities of photons detected, γ', and neutrons detected, ν', following a fission event.

A. Simulation fidelity

To validate the POLIMI model and the detector response model, EJ-309 detector pulse height and time-of-flight distributions are compared to experiment results in Figs. 8–11 using POLIMI. POLIMI was used to transport emitted fragments, neutrons and photons from fission events generated by the three models (POLIMI, CGMF, and FREYA). Because evaluated spectra are used in the POLIMI fission source, Mannhart [39] for neutrons and Valentine [31] for photons, we expect agreement with experiment when the geometrical and detector response models are accurate.

The experimental count rates and pulse heights include only events in a specified time range after the fission start signal. A time window of 15 to 150 ns (energy equivalent of 22 to 0.2 MeV) after the fission events was used for neutrons while, for photons, a time window of 1 to 20 ns after fission was employed. The time regions from −150 to −15 ns and from −20 to −1 ns before the fission start signal were subtracted as background for neutrons and photons respectively since only accidental detections are expected before the fission start signal.

In Figs. 8(a) and 9(a), simulated and experimental pulse height distributions are compared and are shown to agree well over most of the pulse height range. The POLIMI result is within 15% of the experimental result over the entire range for both neutrons and photons. The ratios between the POLIMI and experiment results, C/E, shown in Figs. 8(b) and 9(b), better quantify the agreement. In the neutron pulse height histogram, disagreement above 0.8 MeV is attributed to error in the function to convert proton recoil energy to light output used in the detector response emulator [50]. For photon pulse heights below 0.8 MeV, the simulation underpredicts the count rate. Because low pulse height detections are susceptible to PSD misclassification, some photon events are misclassified as neutron events or vice versa. However, the photon simulations agree within 5% over most of the range. The mean pulse height distributions in Figs. 8(a) and 9(a) show that the POLIMI model, including detector response, accurately replicates the experiment.

In Fig. 10, the simulated neutron time-of-flight distributions agree well with experiment over most of the time range, with the exception of the region below 20 ns. Given the upper (3180 keVee or 8100 keV proton recoil) and the lower (100 keVee or 800 keV proton recoil) pulse height thresholds, most neutron time-of-flight counts are expected between 25 and 80 ns for a fission neutron spectrum. The experiment is susceptible to particle misclassification, particularly evident

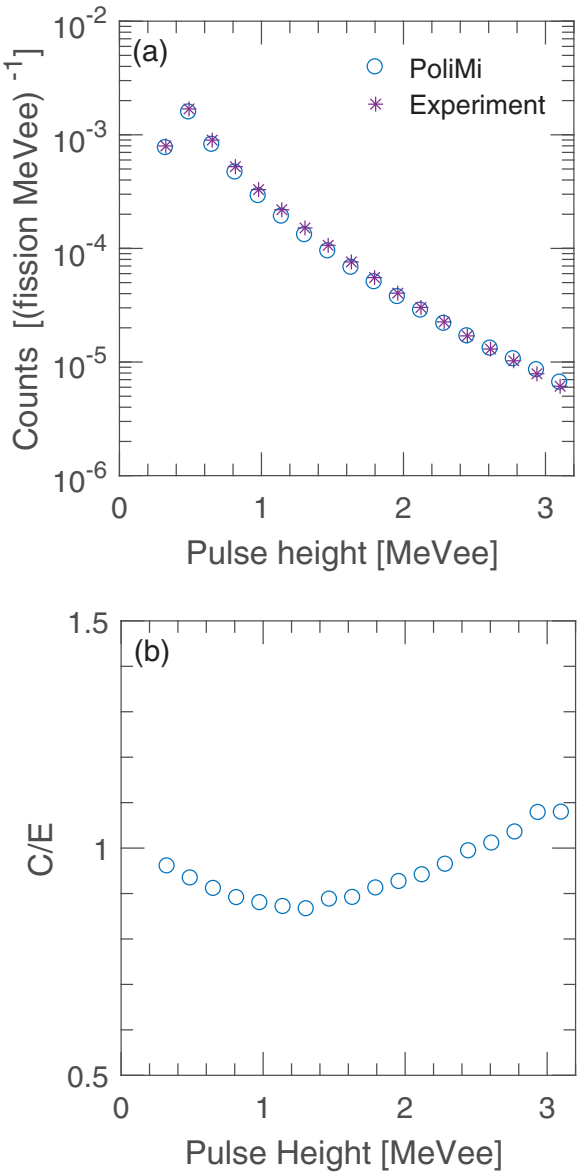

FIG. 8. Calculated and experimental mean pulse height neutron distributions (a) and the ratio of the calculation results to the measurement, C/E (b), are shown. The results are averaged over all detectors. The statistical uncertainties are smaller than the points. Approximately 6.1×10^6 detections are shown for the experimental results.

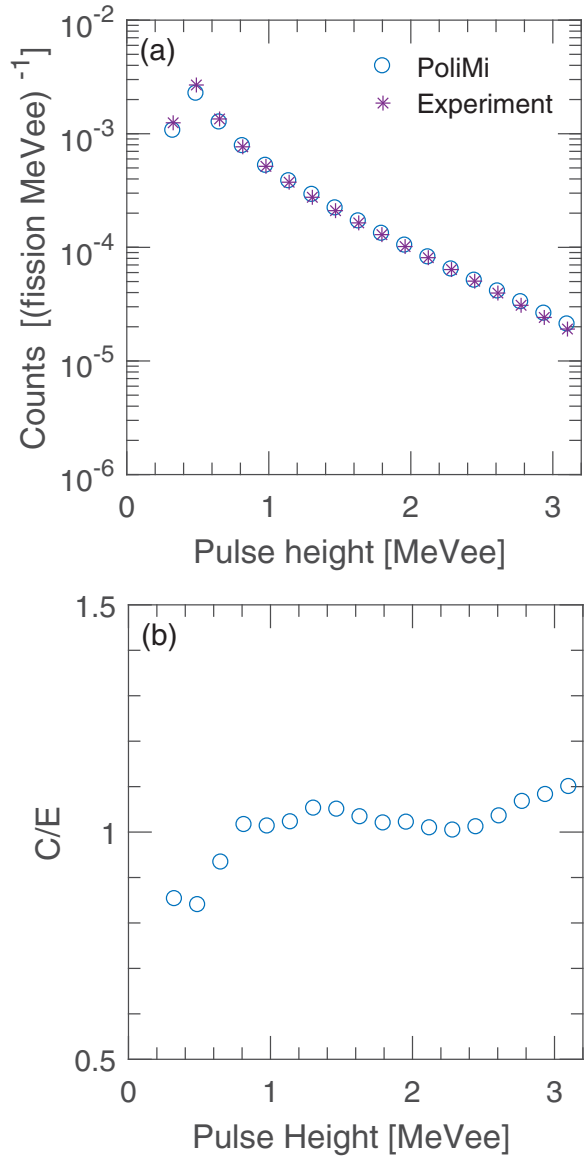

FIG. 9. Calculated and experimental mean pulse height photon distributions (a) and the ratio of the calculation results to the measurement, C/E (b), are shown. The results are averaged over all detectors. The statistical uncertainties are smaller than the points. Approximately 1×10^7 detections are shown for the experimental results.

below 20 ns, whereas the simulated particle identification is perfect. For $30 < \Delta t < 75$ ns, POLIMI agrees with experiment within 10%. A small peak is seen in Fig. 10(b) in C/E in this region because fast neutrons arriving at the detector induce photons in the active volume of the detector and some neutrons may be misclassified as photons. Above 75 ns, room return becomes significant and C/E decreases. In Fig. 11, the simulated and measured photon time-of-flight distributions agree well over most of the time range except for $\Delta t > 75$ ns, where the model overestimates room return.

Agreement within 10% is considered sufficient confidence that the measurement and simulation agree, and further analysis of higher-order coincidence and correlation results using simulations may be performed with confidence. The POLIMI simulation agrees with experiment, as expected, because the built-in model uses evaluated multiplicity and energy spectra. The close agreement between the simulation and measurement for the pulse height and time-of-flight distributions provides confidence in the model of the laboratory and the detector response.

B. Correlated fission model comparisons

Comparisons between the simulated and experimental pulse height, time-of-flight, and coincidence distributions are shown for each fission model to demonstrate the effect of detector

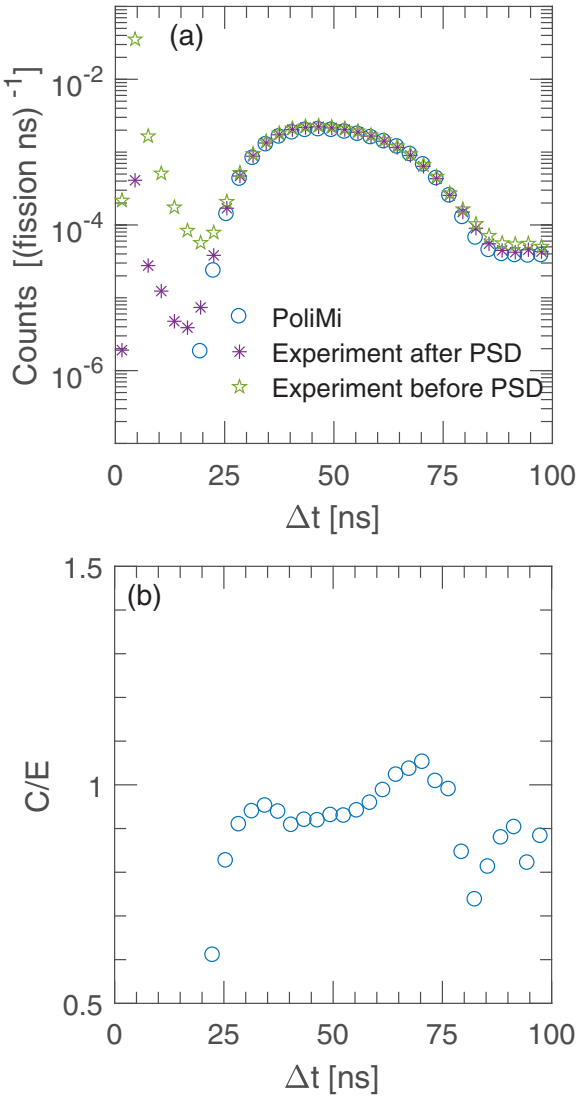

FIG. 10. (a) The calculated and experimental neutron time-of-flight distributions. The experimental distribution after background subtraction is shown before and after PSD. (b) The ratio of the calculation to the measurement after PSD, C/E. The results are averaged over all detectors. Time zero was the time of the fission start signal. The uncertainties are smaller than the points: 3.6×10^6 detections are shown for the experimental result.

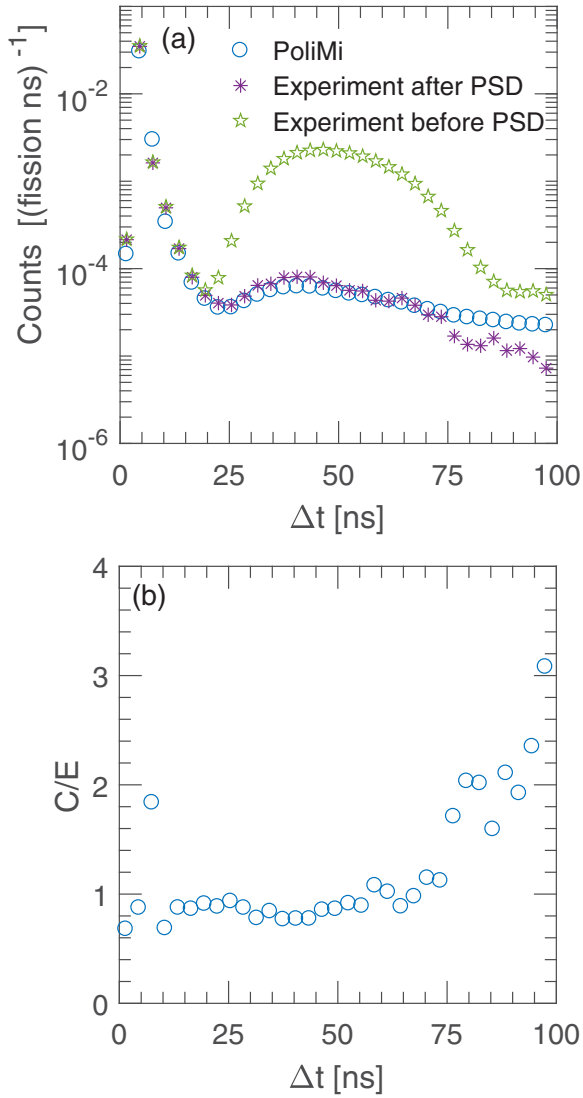

FIG. 11. (a) The calculated and experimental photon time-of-flight distributions. The experimental distribution after background subtraction is shown before and after PSD. (b) The ratio of the calculation to the measurement after PSD, C/E. The results are averaged over all detectors. Time zero was the time of the fission start signal. The uncertainties are smaller than the points; 6.2×10^6 detections are shown for the experimental result.

response on each model and to highlight the differences between the models. Joint-particle distributions are then compared to evaluate the correlation and the effect of neutron and photon competition during fragment deexcitation in experiment and simulation. Differences between the models may be expected in both single- and interparticle distributions.

The CGMF and the FREYA photon and neutron pulse height histograms do not agree well with experiment, as shown in Figs. 12 and 13. CGMF underestimates neutron pulse heights over the sensitive range and FREYA overestimates over most of the range, especially at high pulse heights. This indicates that the CGMF neutron spectrum is too soft while the FREYA prompt fission neutron spectrum is too hard in the measured energy range. These calculation results are consistent with the emission data in Fig. 3(a), where the CGMF result is softer than the evaluation and FREYA is harder than the evaluation. The good agreement with POLIMI is because the model uses the evaluated spectrum.

The photon pulse height histograms, however, show that the CGMF distribution is uniformly too high above 1 MeVee, and FREYA, while lower than CGMF, increasingly overestimates toward higher pulse heights. This indicates that both CGMF and FREYA produce too many high energy photons. Both the CGMF and the FREYA photon energy spectra are higher than the POLIMI spectrum toward higher energies in Fig. 3(b). Again, the POLIMI model, using evaluated spectra, shows expected good agreement.

The CGMF and FREYA neutron time-of-flight distributions in Fig. 14 exhibit poorer agreement than the POLIMI built-in

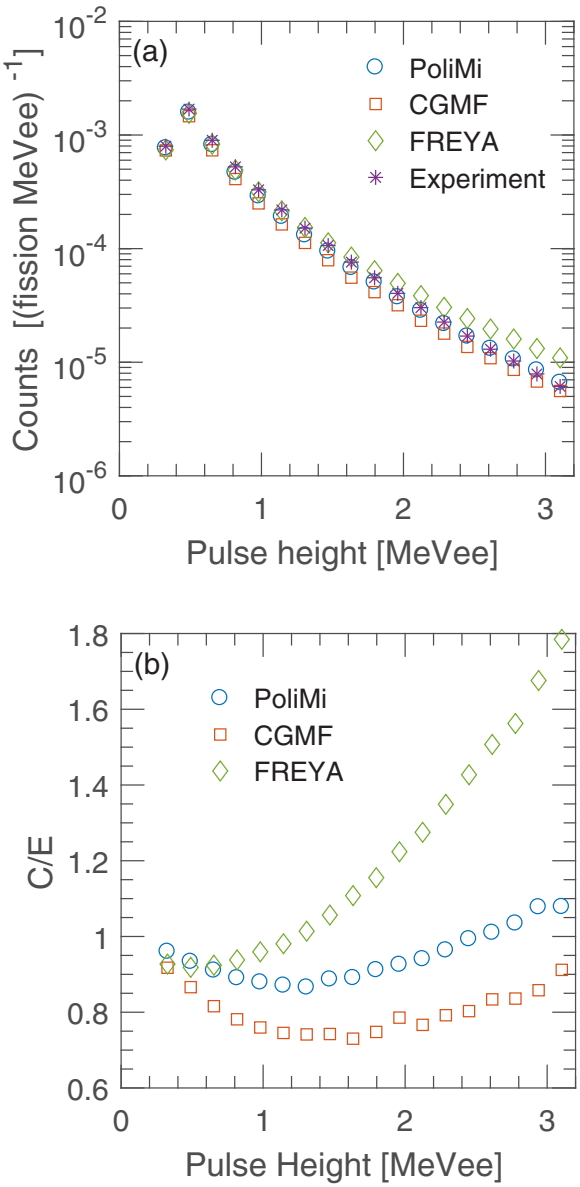

FIG. 12. (a) The calculated and experimental neutron pulse height distributions. (b) The ratio of the calculation to the measurement, C/E. The results are averaged over all detectors. The uncertainties are smaller than the points; 6.1×10^6 detections are shown for the experimental result.

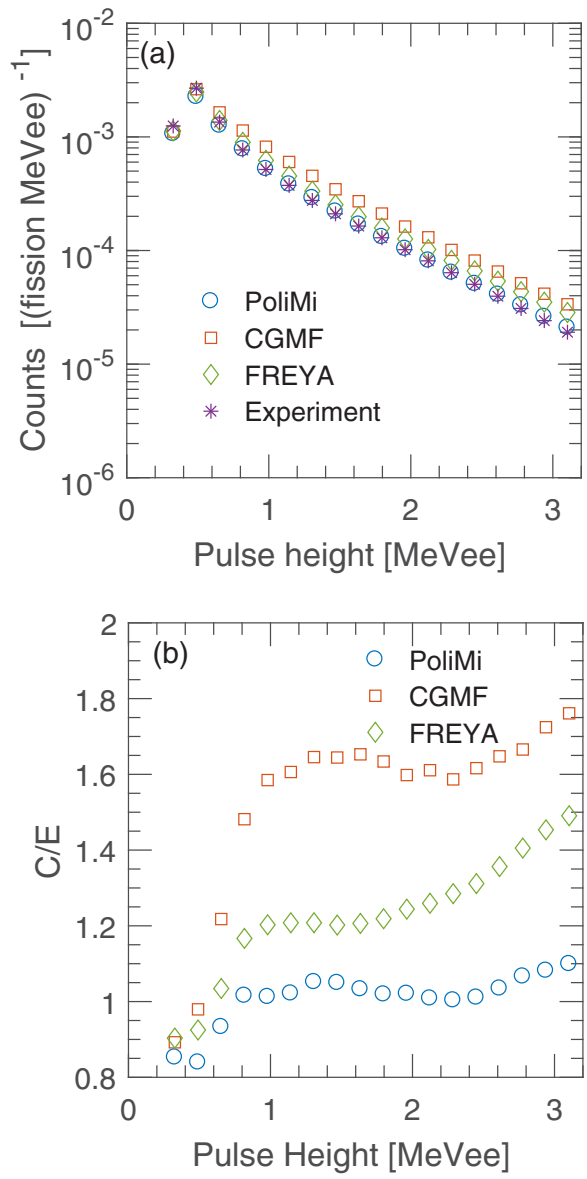

FIG. 13. (a) The calculated and experimental photon pulse height distributions. (b) The ratio of the calculation to the measurement, C/E. The results are averaged over all detectors. The uncertainties are smaller than the points; 1×10^7 detections are shown for the experimental result.

model. FREYA produces too many fast neutrons while CGMF has too few fast neutrons and too many slower neutrons. This result is consistent with the harder FREYA neutron spectrum and with the softer CGMF neutron spectrum relative to the evaluation, shown in Fig. 3(a).

The POLIMI, CGMF, and FREYA photon time-of-flight distributions in Fig. 15 show similar agreement below 10 ns while CGMF and FREYA show poorer agreement above 18 ns than POLIMI. Above 18 ns, delayed, scattered, and fast-neutron induced photons contribute to the signal. The POLIMI model produces time-distributed photons where a small fraction of photons are delayed according to Maier-Leibnitz *et al.* [51], whereas the CGMF and FREYA photon emissions only include prompt emission. The POLIMI result agrees between 18 and 75 ns because of a small contribution of delayed photons, but beyond 75 ns POLIMI produces too many delayed photons. The region between 18 and 75 ns could also include a small contribution from neutrons misclassified as photons.

On a event-by-event basis, neutron coincidence distributions are shown in Fig. 16. The coincidence distribution is a convolution of the emitted multiplicity and the detector system response. Therefore, given the efficiency of the detection system, $\overline{\nu'}$, the mean number of detected neutrons, is expected to be much less than $\overline{\nu}$, and $\overline{\gamma'}$, the mean number of detected photons, is also expected to be much less than $\overline{\gamma}$. The neutron coincidences in FREYA agree well with experiment, as shown

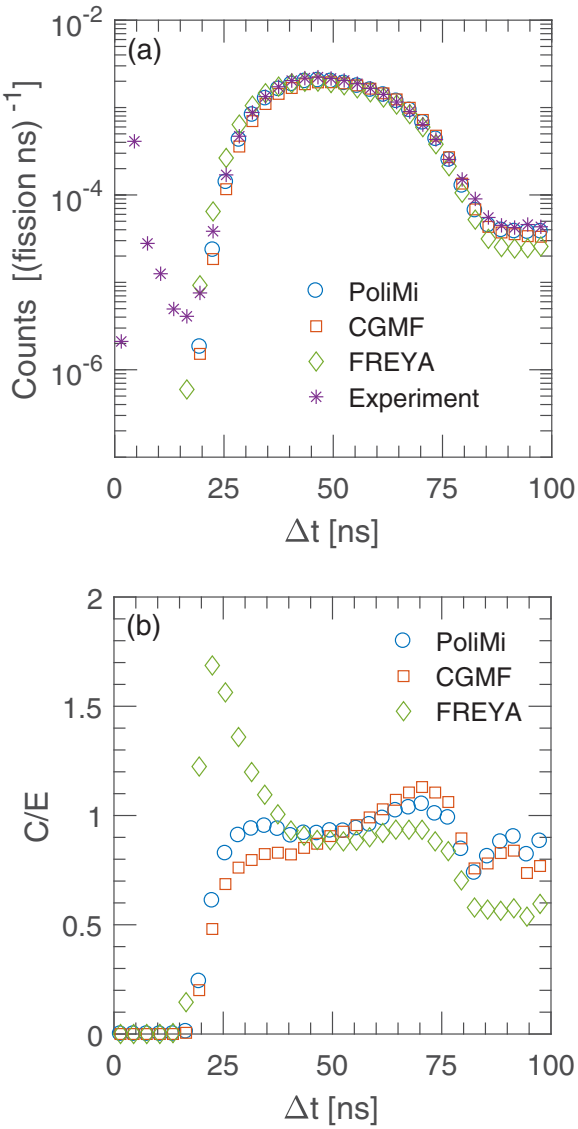

FIG. 14. (a) The calculated and experimental neutron time-of-flight distributions. (b) The ratio of the calculation to the measurement, C/E. The results are averaged over all detectors. The uncertainties are smaller than the points; 3.6×10^6 detections are shown for the experimental result.

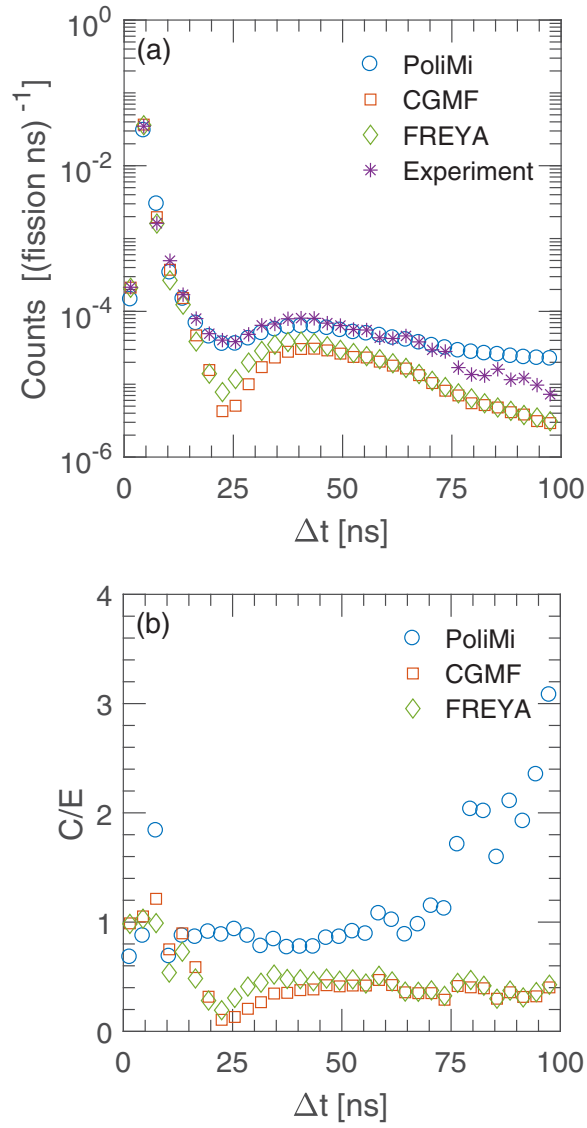

FIG. 15. (a) The calculated and experimental photon time-of-flight distributions. (b) The ratio of the calculation to measurement, C/E. The results are averaged over all detectors. The uncertainties are smaller than the points; 6.2×10^6 detections are shown for the experimental result.

by the C/E for all ν' close to unity. Agreements of CGMF and POLIMI are similarly poor, overestimating C/E for more than two neutrons in coincidence, despite the CGMF $\overline{\nu}$ being higher than that for POLIMI.

The photon coincidence distributions are shown in Fig. 17. Photon coincidences from POLIMI agree well with experiment. Here CGMF overestimates the number of photon coincidences over the whole range while FREYA underestimates $P(\gamma')$ for $\gamma' > 2$. While POLIMI and FREYA have similar $\overline{\gamma}$, shown in Fig. 4(b), the impact of the narrower full photon multiplicity of FREYA shows at higher coincidences.

C. Correlations between neutrons and photons

Figure 18 compares the calculated $E[\gamma'|\nu']$, the expected number of photons detected given the number of neutrons detected, as a function of ν' to the experimental result. $E[\gamma'|\nu']$ and $E[\nu'|\gamma']$, the number of neutrons detected given the number of photons detected (shown in Fig. 19), are corrected for detector dead time as more particles are detected.

Figure 18 indicates little to no correlation for POLIMI and negative correlation for the other results. The POLIMI model is uncorrelated, therefore the result is expected to be invariant with neutron coincidences. The negative multiplicity correlation in CGMF and FREYA gives the expected result of decreased $E[\gamma'|\nu']$ for increasing ν'. This trend, however, is weak. In particular, since $\nu' = 4$ is greater than the measured $\overline{\nu}$ for ^{252}Cf(sf), ~3.76, the uncertainty on the model calculations, combined with the detector efficiencies, leads to large uncertainties on $E[\gamma'|\nu']$ for this value of ν'.

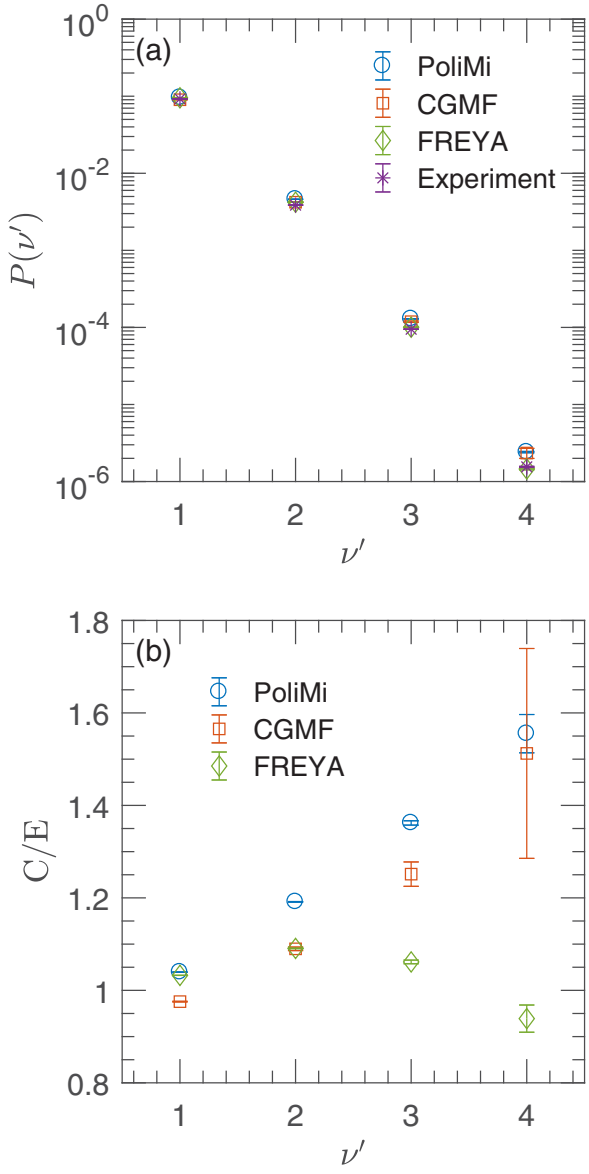

FIG. 16. (a) Detected neutron multiplicity distribution, $P(\nu')$, after fission. (b) Calculated results relative to experiment. There are 3.3×10^8 neutron detections in the experimental result. Error bars represent statistical uncertainty only.

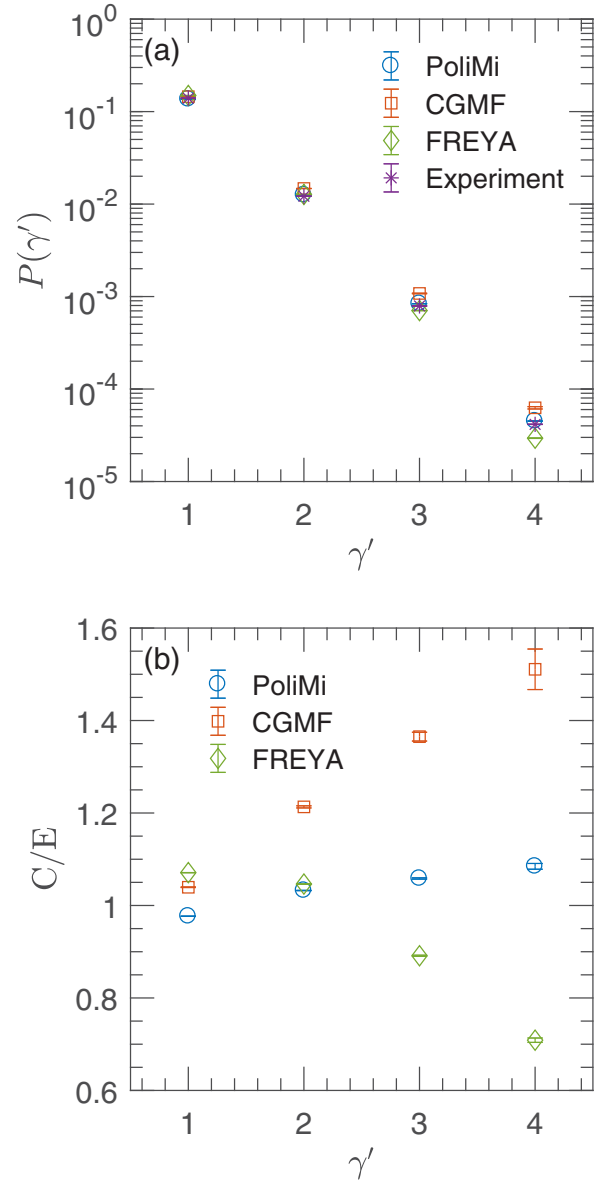

FIG. 17. (a) Detected photon multiplicity distribution, $P(\gamma')$, after fission. (b) Calculated results relative to experiment. There are 5.6×10^8 photon detections in the experimental result. Error bars represent statistical uncertainty only.

Figure 19 shows the relationship between $E[\nu'|\gamma']$ and γ' for the experiment and the simulations. Little to no correlation in POLIMI was observed while a negative correlation is seen for CGMF and FREYA, similar to the result in Fig. 18, albeit with a clearer trend in the zoom of $E[\nu'|\gamma']$ in Fig. 19(b), as expected. Here $\gamma' = 4$ is less than the measured average photon multiplicity for ^{252}Cf(sf), ~7.98 [33]. Thus one might expect the simulations to have smaller uncertainties for this value of γ', as shown in Fig. 19. The larger CGMF uncertainty on both $\nu' = 4$ and $\gamma' = 4$ in Figs. 18 and 19 is due to the reuse of events from the history file.

We now discuss how the results compare to those of previous experiments. Recall that Glässel *et al.* found a negative neutron and photon multiplicity correlation of 0.02 neutrons per photon [14] on an event-by-event basis while Nifenecker *et al.* [12] suggested a positive correlation of 0.89 neutrons per photon. To place these results on Fig. 19, a simple forward model was employed to propagate them through an analytic correlation model including detector response.

The analytic model assumed that both the neutron and the photon energy spectra were invariant with multiplicity, a binomial neutron multiplicity distribution [49], a double Poisson photon multiplicity distribution [33], and linear correlation between neutron and photon multiplicity. The photon spectrum is known to soften as photon multiplicity increases [52]. Assuming an invariant photon spectrum would only result in a small bias because the organic scintillators are sensitive to the full photon spectrum.

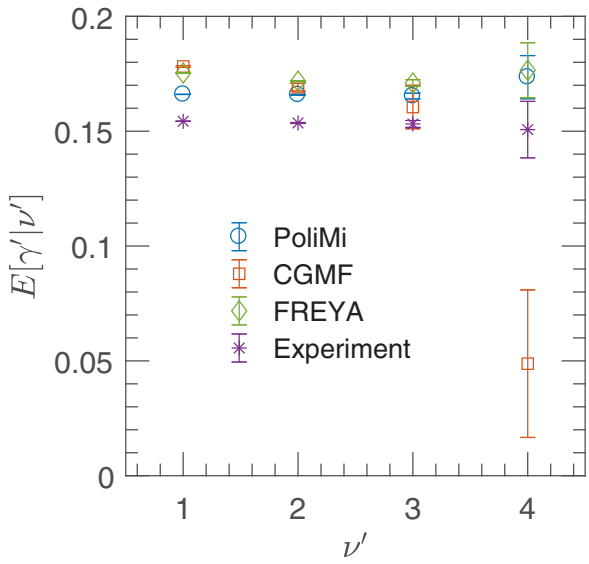

FIG. 18. Expected number of detected photons given ν' neutrons detected in coincidence, $E[\gamma'|\nu']$. The experimental data include 7.8×10^8 detected fission events. Error bars represent statistical uncertainty only.

The photon multiplicity distribution $\Pi(G)$ for G prompt photons emitted was assumed to be a double Poisson distribution [33],

$$\Pi(G) = C_1 \frac{(C_2)^G e^{-C_2}}{G!} + (1 - C_1)\frac{(C_3)^G e^{-C_3}}{G!}, \qquad (3)$$

where $C_1 = 0.675$, $C_2 = 6.78$, and $C_3 = 9.92$ [33]. The neutron and photon multiplicities were assumed to be linearly correlated. In the forward model, the photon distribution, Eq. (3), was assumed to be unchanged while the neutron multiplicity was adjusted by linearly varying the average number of neutrons emitted, $\overline{\nu}$, for a fixed photon multiplicity G. The neutron multiplicity distribution was assumed to be binomial [49] with emission of up to $m = 9$ neutrons allowed,

$$P(\nu) = \frac{m!}{\nu!(m-\nu)!}\left(\frac{\overline{\nu}}{m}\right)^{\nu}\left(1 - \frac{\overline{\nu}}{m}\right)^{m-\nu}. \qquad (4)$$

The neutron and photon efficiencies simulated by POLIMI were applied to the emitted photon and neutron distributions to produce $E[\nu'|\gamma']$ as a function of γ' for the Nifenecker and Glässel correlations, $+0.89$ and -0.02 $\overline{\nu}$ per emitted photon, respectively. The agreement between the experimental result and Nifenecker *et al.* in Fig. 19 is poor. Nifenecker *et al.* lies above the experiment data and all simulations with the discrepancy increasing with γ'. This poor agreement suggests that the positive multiplicity correlation binned with fragment properties observed by Nifenecker does not predict neutron-photon competition on an event-by-event basis. Thus the strong positive correlation suggested by Nifenecker is excluded by our result. Figure 19(b) omits the Nifenecker result to show low $E[\nu'|\gamma']$ to separate other results.

The Glässel correlation, however, shows a slightly negative trend in $E[\nu'|\gamma']$, smaller than the trends of CGMF, FREYA, and our experimental result.

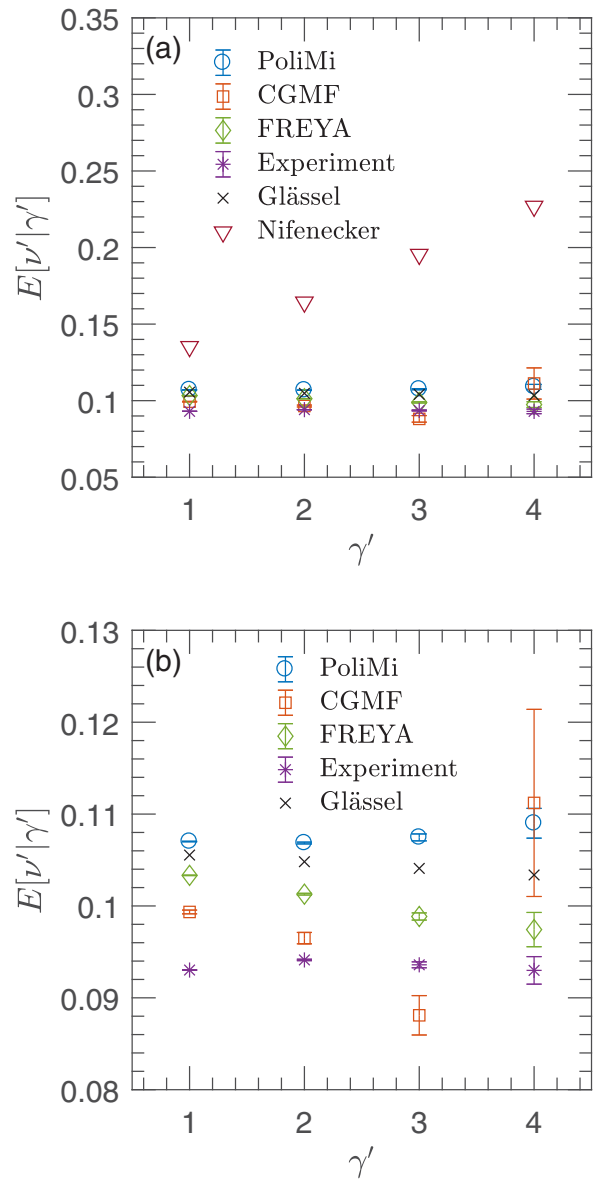

FIG. 19. Expected number of detected neutrons given γ' photons detected in coincidence, (a) $E[\nu'|\gamma']$, and zoomed in to separate the results at low $E[\nu'|\gamma']$ (b). The experimental data include 7.8×10^8 detected fission events. Error bars represent statistical uncertainty only.

Using a linear fit to the $E[\nu'|\gamma']$ data and the correlation model outlined in Eqs. (3) and (4), the experimental result shows a slight negative correlation of -0.0016 ± 0.0096 $\overline{\nu}$ per emitted photon. This result indicates a weaker neutron-photon correlation than the Glässel result, also weaker than the CGMF and FREYA results. The Bleuel *et al.* data [15], based on measurements of the photon multiplicity distribution with two and four neutrons emitted from Mo/Ba fragment pairs, indicated little to no correlation. However, the Bleuel *et al.* experiment may have been insensitive to the weak correlation measured here. Additionally, it is not clear how selecting fragments with specific neutron multiplicities might bias the result of Ref. [15].

Calculated relative to experiment data, C/E, shown in Figs. 12–15, demonstrate some uncertainty in the detector response, both in calculations and in experiment. We expect the uncertainty in detector response to manifest as a discrepancy in the expected magnitude of the calculated $E[\nu'|\gamma']$ or $E[\gamma'|\nu']$ data, but we do not expect uncertainty to affect in the overall trend or correlation of the data. Therefore, the comparisons of experiment and calculated trends in $E[\nu'|\gamma']$ or $E[\gamma'|\nu']$ are reliable. If, however, there were energy-multiplicity correlations that produced strong spectral shifts outside of the sensitive range of the detectors, then the trends in $E[\nu'|\gamma']$ and $E[\gamma'|\nu']$ could be unreliable. However, the detectors should be sensitive to most energy-multiplicity correlations; as stated before, the detectors are estimated to be sensitive to 77% of the ^{252}Cf(sf) neutron spectrum and to the full photon spectrum.

VI. CONCLUSIONS

A dedicated experiment to observe neutron-photon multiplicity correlations in ^{252}Cf(sf) was performed and compared to simulations using correlated emission fission models. The experiment showed a weak negative neutron-photon multiplicity correlation on an event-by-event basis of -0.0016 ± 0.0096 $\bar{\nu}$ per emitted photon for ^{252}Cf(sf). This result suggests weak competition between neutron and photon emission.

The simulated results for all employed models agree well with the pulse height and the time-of-flight distributions. Comparison of the experiment and the `POLIMI` simulation results show that `MCPNX-PoliMi` with `CGMF` and `FREYA` generated events best explain the neutron-photon multiplicity correlation because of their inherent negative correlation. The correlation in the `CGMF` and `FREYA` models, however, is stronger than observed in the experiment.

Future work should include experiments that simultaneously measure fragment properties and emissions with high efficiency. Higher neutron and photon efficiency would allow for a more sensitive measurement of the multiplicity correlation. Event-by-event correlations measured with respect to TKE would help to understand how excitation and spin impact emission competition. Additionally, experiments should include measurements of event-by-event energy correlations.

ACKNOWLEDGMENTS

This work was performed under the auspices of the U.S. Department of Energy by Los Alamos National Security, LLC, under Contract No. DE-AC52-06NA25396, by Lawrence Livermore National Security, LLC, under Contract No. DE-AC52-07NA27344, by the Consortium for Verification Technology under Contract No. DE-NA0002534, and by the Office of Nuclear Physics in the Office of Science under Contract No. DE-AC02-05CH11231.

[1] J. S. Fraser, The angular distribution of prompt neutrons emitted in fission, Phys. Rev. **88**, 536 (1952).
[2] K. Skarsvag, Time distribution of gamma-rays from spontaneous fission of ^{252}Cf, Nucl. Phys. A **153**, 82 (1970).
[3] H. R. Bowman, S. G. Thompson, J. C. D. Milton, and W. J. Swiatecki, Velocity and angular distributions of prompt neutrons from spontaneous fission of Cf^{252}, Phys. Rev. **126**, 2120 (1962).
[4] P. Santi and M. Miller, Reevaluation of prompt neutron emission multiplicity distributions for Spontaneous fission, Nucl. Sci. Eng. **160**, 190 (2008).
[5] A. S. Vorobyev, O. A. Shcherbakov, A. M. Gagarski, G. V. Val'ski, and G. A. Petrov, Investigation of the prompt neutron emission mechanism in low energy fission of ^{235,233}U(n_{th},f) and ^{252}Cf(sf), EPJ Web Conf. **8**, 03004 (2010).
[6] J. L. Ullmann, E. M. Bond, T. A. Bredeweg, A. Couture, R. C. Haight, M. Jandel, T. Kawano, H. Y. Lee, J. M. O'Donnell, A. C. Hayes, I. Stetcu, T. N. Taddeucci, P. Talou, D. J. Vieira, J. B. Wilhelmy, J. A. Becker, A. Chyzh, J. Gostic, R. Henderson, E. Kwan, and C. Y. Wu, Prompt γ-ray production in neutron-induced fission of ^{239}Pu, Phys. Rev. C **87**, 044607 (2013).
[7] E. Kwan, C. Y. Wu, R. C. Haight, H. Y. Lee, T. A. Bredeweg, A. Chyzh, M. Devlin, N. Fotiades, J. M. Gostic, R. A. Henderson, M. Jandel, A. Laptev, R. O. Nelson, J. M. O'Donnell, B. A. Perdue, T. N. Taddeucci, J. L. Ullmann, and S. A. Wender, Prompt fission γ-rays measured using liquid scintillators, Nucl. Data Sheets **119**, 221 (2014).
[8] V. N. Dushin, F.-J. Hambsch, V. A. Jakovlev, V. A. Kalinin, I. S. Kraev, A. B. Laptev, D. V. Nikolaev, B. F. Petrov, G. A. Petrov, V. I. Petrova, Y. S. Pleva, O. A. Shcherbakov, V. I. Shpakov, V. E. Sokolov, A. S. Vorobyev, and T. A. Zavarukhina, Facility for neutron multiplicity measurements in fission, Nucl. Instrum. Methods Phys. Res., Sect. A **516**, 539 (2004).
[9] R. Billnert, F.-J. Hambsch, A. Oberstedt, and S. Oberstedt, New prompt spectral γ-ray data from the reaction ^{252}Cf(sf) and its implication on present evaluated nuclear data files, Phys. Rev. C **87**, 024601 (2013).
[10] A. Göök, F.-J. Hambsch, and M. Vidali, Prompt neutron multiplicity in correlation with fragments from spontaneous fission of ^{252}Cf, Phys. Rev. C **90**, 064611 (2014).
[11] A. Oberstedt, R. Billnert, F.-J. Hambsch, and S. Oberstedt, Impact of low-energy photons on the characteristics of prompt fission γ-ray spectra, Phys. Rev. C **92**, 014618 (2015).
[12] H. Nifenecker, C. Signarbieux, M. Ribrag, J. Poitou, and J. Matuszek, Gamma-neutron competition in the de-excitation mechanism of the fission fragments of ^{252}Cf, Nucl. Phys. A **189**, 285 (1972).
[13] T. Wang, G. Li, L. Zhu, Q. Meng, L. Wang, H. Han, W. Zhang, H. Xia, L. Hou, R. Vogt, and J. Randrup, Correlations of neutron multiplicity and γ-ray multiplicity with fragment mass and total kinetic energy in spontaneous fission of ^{252}Cf, Phys. Rev. C **93**, 014606 (2016).
[14] P. Glässel, R. Schmid-Fabian, D. Schwalm, D. Habs, and H. U. V. Helmolt, ^{252}Cf fission revisited–new insights into the fission process, Nucl. Phys. A **502**, 315 (1989).
[15] D. L. Bleuel, L. A. Bernstein, J. T. Burke, J. Gibelin, M. D. Heffner, J. Mintz, E. B. Norman, L. Phair, N. D. Scielzo, S. A. Sheets, N. J. Snyderman, M. A. Stoyer, and M. Wiedeking, Gamma-ray multiplicity measurement of the spontaneous fission of ^{252}Cf in a segmented HPGe/BGO detector array, Nucl. Instrum. Methods Phys. Res., Sect A **624**, 691 (2010).
[16] P. Talou, T. Kawano, and I. Stetcu, Monte Carlo Hauser-Feshbach Calculations of Prompt Fission Neutrons and Gamma Rays: Application to Thermal Neutron-Induced Fission

Reactions on U-235 and Pu-239, Los Alamos National Laboratory Technical Report No. LA-UR-12-25059, 2012 (unpublished).
[17] P. Talou, T. Kawano, and I. Stetcu, Prompt fission neutrons and gamma rays in a Monte Carlo Hauser-Feshbach formalism, Phys. Procedia **47**, 39 (2013).
[18] P. Talou, I. Stetcu, and T. Kawano, Modeling the emission of prompt fission γ rays for fundamental physics and applications, Phys. Procedia **59**, 83 (2014).
[19] P. Talou, T. Kawano, I. Stetcu, J. P. Lestone, E. McKigney, and M. B. Chadwick, Late-time emission of prompt fission γ rays, Phys. Rev. C **94**, 064613 (2016).
[20] J. Randrup and R. Vogt, Calculation of fission observables through event-by-event simulation, Phys. Rev. C **80**, 024601 (2009).
[21] R. Vogt and J. Randrup, Event-by-event study of neutron observables in spontaneous and thermal fission, Phys. Rev. C **84**, 044621 (2011).
[22] R. Vogt and J. Randrup, Event-by-event study of neutron observables in spontaneous and thermal fission, Phys. Rev. C **87**, 044602 (2013).
[23] R. Vogt and J. Randrup, Neutron angular correlations in spontaneous and neutron-induced fission, Phys. Rev. C **90**, 064623 (2014).
[24] J. Randrup and R. Vogt, Refined treatment of angular momentum in the event-by-event fission model FREYA, Phys. Rev. C **89**, 044601 (2014).
[25] R. Vogt and J. Randrup, Improved modeling of photon observables with the event-by-event fission model FREYA, Phys. Rev. C **96**, 064620 (2017).
[26] J. M. Verbeke, J. Randrup, and R. Vogt, Fission reaction event yield Algorithm FREYA 2.0.2, Comput. Phys. Commun. **222**, 263 (2018).
[27] C. Wagemans, *The Nuclear Fission Process* (CRC, Boca Raton, FL, 1991), pp. 498–501.
[28] F. S. Dietrich, J. C. Browne, W. J. O'Connell, and M. J. Kay, Spectrum of γ rays in the 8- to 20-MeV range from ^{252}Cf spontaneous fission, Phys. Rev. C **10**, 795 (1974).
[29] S. A. Pozzi, E. Padovani, and M. Marseguerra, MCNP-PoliMi: A Monte-Carlo code for correlation measurements, Nucl. Instrum. Methods Phys. Res., Sect A **513**, 550 (2003).
[30] S. A. Pozzi, S. D. Clarke, W. J. Walsh, E. C. Miller, J. L. Dolan, M. Flaska, B. M. Wieger, A. Enqvist, E. Padovani, J. K. Mattingly, D. L. Chichester, and P. Peerani, MCNPX-PoliMi for nuclear nonproliferation applications, Nucl. Instrum. Methods Phys. Res., Sect A **694**, 119 (2012).
[31] T. E. Valentine and J. T. Mihalczo, MCNP-DSP: A neutron and gamma ray Monte Carlo calculation of source-driven noise-measured parameters, Ann. Nucl. Energy **23**, 1271 (1996).
[32] D. G. Madland and J. R. Nix, New calculation of prompt fission neutron spectra and average prompt neutron multiplicities, Nucl. Sci. Eng. **81**, 213 (1982).
[33] T. E. Valentine, Evaluation of prompt fission gamma rays for use in simulating nuclear safeguard measurements, Ann. Nucl. Energy **28**, 191 (2001).
[34] O. Litaize, O. Serot, and L. Berge, Fission modeling with FIFRELIN, Eur. Phys. J. A **51**, 177 (2015).
[35] K. H. Schmidt, B. Jurado, C. Amouroux, and C. Schmitt, General description of fission observables: GEF model code, Nucl. Data Sheets **131**, 107 (2016).
[36] S. A. E. Johansson, Gamma de-excitation of fission fragments: (I). Prompt radiation, Nucl. Phys. **60**, 378 (1964).
[37] S. A. E. Johansson, Gamma de-excitation of fission fragments: (II). Delayed radiation, Nucl. Phys. **64**, 147 (1965).
[38] W. John, J. J. Wesolowski, and F. Guy, Mass-dependent structure in the fission γ-ray yields from ^{252}Cf, Phys. Lett. B **30**, 340 (1969).
[39] W. Mannhart, Evaluation of the Cf-252 fission neutron spectrum between 0 MeV and 20 MeV, in *Properties of Neutron Sources*, Proceedings of an Advisory Group Meeting, Leningrad, 9–13 June 1985 (IAEA, Vienna, 1987), pp. 158–171.
[40] P. Talou, R. Vogt, J. Randrup, M. E. Rising, J. Verbeke, M. T. Andrews, S. D. Clarke, P. Jaffke, M. Jandel, T. Kawano, M. J. Marcath, K. Meierbachtol, G. Rusev, A. Sood, I. Stetcu, and C. Walker, Correlated prompt fission data in transport simulations, Eur. Phys. J. A **54**, 9 (2018).
[41] R. C. Haight, H. Y. Lee, T. N. Taddeucci, J. M. O'Donnell, B. A. Perdue, N. Fotiades, M. Devlin, J. L. Ullmann, A. Laptev, T. Bredeweg, M. Jandel, R. O. Nelson, S. A. Wender, M. C. White, C. Y. Wu, E. Kwan, A. Chyzh, R. Henderson, and J. Gostic, The prompt fission neutron spectrum (PFNS) measurement program at LANSCE, Nucl. Data Sheets **119**, 205 (2014).
[42] L. E. Kirsch, M. Devlin, S. M. Mosby, and J. A. Gomez, A new measurement of the ^{6}Li(n,α)t cross section at MeV energies using a ^{252}Cf fission chamber and ^{6}Li scintillators, Nucl. Instrum. Methods Phys. Res., Sect A **874**, 57 (2017).
[43] R. B. Oberer, Maximum Alpha To Minimum Fission Pulse Amplitude for a Parallel- Plate and Hemispherical Cf-252 Ion-Chamber Instrumented Neutron Source, Oak Ridge National Laboratory Technical Report No. ORNL/TM-2000/290, 2000 (unpublished).
[44] N. J. Roberts and L. N. Jones, The content of ^{250}Cf and ^{248}Cm in ^{252}Cf neutron sources and the effect on the neutron emission rate, Radiat. Prot. Dosimetry **126**, 83 (2007).
[45] F. D. Brooks, R. W. Pringle, and B. L. Funt, Pulse shape discrimination in a plastic scintillator, IRE Trans. Nucl. Sci. **7**, 35 (1960).
[46] L. F. Miller, J. Preston, S. Pozzi, M. Flaska, and J. Neal, Digital pulse shape discrimination, Radiat. Prot. Dosimetry **126**, 253 (2007).
[47] M. M. Bourne, S. D. Clarke, N. Adamowicz, S. A. Pozzi, N. Zaitseva, and L. Carman, Neutron detection in a high-gamma field using solution-grown stilbene, Nucl. Instrum. Methods Phys. Res., Sect A **806**, 348 (2016).
[48] J. K. Polack, M. Flaska, A. Enqvist, C. S. Sosa, C. C. Lawrence, and S. A. Pozzi, An algorithm for charge-integration, pulse-shape discrimination and estimation of neutron/photon misclassification in organic scintillators, Nucl. Instrum. Methods Phys. Res., Sect A **795**, 253 (2015).
[49] B. C. Diven, H. C. Martin, R. F. Taschek, and J. Terrell, Multiplicities of Fission Neutrons, Phys. Rev. **101**, 1012 (1956).
[50] M. A. Norsworthy, A. Poitrasson-Rivière, M. L. Ruch, S. D. Clarke, and S. A. Pozzi, Evaluation of neutron light output response functions in EJ-309 organic scintillators, Nucl. Instrum. Methods Phys. Res., Sect A **842**, 20 (2017).
[51] H. Maier-Leibnitz, P. Armbruster, and H. J. Specht, Prompt and delayed gamma-rays from fission, in *Physics and Chemistry of Fission*, Proceedings of the Symposium, Salzburg, 1965, 1965 (IAEA, Vienna, 1965), pp. 113–123.
[52] I. Stetcu, P. Talou, T. Kawano, and M. Jandel, Properties of prompt-fission γ rays, Phys. Rev. C **90**, 024617 (2014).

Correction: The first sentence of Sec. IV A contained a production error and has been fixed.